Mid-IR Supercontinuum Generation From Nonsilica Microstructured Optical Fibers

Jonathan H. V. Price, *Member, IEEE*, Tanya M. Monro, Heike Ebendorff-Heidepriem, Francesco Poletti, Peter Horak, Vittoria Finazzi, Julie Y. Y. Leong, Periklis Petropoulos, Joanne C. Flanagan, Gilberto Brambilla, Xian Feng, and David J. Richardson

***Abstract*—In this paper, the properties of nonsilica glasses and the related technology for microstructured fiber fabrication are reviewed. Numerical simulation results are shown using the properties of nonsilica microstructured fibers for mid-infrared (mid-IR) supercontinuum generation when seeding with near-IR, 200-fs pump pulses. In particular, bismuth glass small-core fibers that have two zero-dispersion wavelengths (ZDWs) are investigated, and efficient mid-IR generation is enabled by phase-matching of a 2.0-μm seed across the upper ZDW into the 3–4.5 μm wavelength range. Fiber lengths considered were 40 mm. Simulation results for a range of nonsilica large-mode fibers are also shown for comparison.**

***Index Terms*—Infrared, microstructured fibers, nonlinear fiber optics, supercontinuum.**

I. Introduction

THERE ARE MANY applications for broad-bandwidth infrared laser sources, including optical frequency metrology [1] and optical tomography [2], and moving into the mid-infrared (mid-IR) sources, uses for wavelengths beyond 2 μm include light-imaging detection and ranging (LIDAR), molecular spectroscopy, and active hyperspectral imaging. Current mid-IR sources are typically based on optical parametric oscillators (OPO) or quantum cascaded lasers (QCL). While OPOs achieve excellent performance, they require large lasers and can be rather complex and costly to maintain, and QCLs are hard to scale up in power. It is, therefore, important to consider if new technology in related areas could be used to create practical, robust, and lower cost mid-IR sources for the future.

Since microstructured optical fibers (MOF) first enabled visible supercontinuum generation using seed pulses directly from a Ti:sapphire oscillator [3], there has been tremendous progress toward explaining this remarkable spectral broadening [4]–[6] and in the development of further applications of these fibers [7]. The use of MOF for supercontinuum generation is particularly attractive since tight mode confinement can be realized, increasing fiber nonlinearity, and because the zero-dispersion wavelength (ZDW) can be tailored to maximize supercontinuum generation for a given pump wavelength.

Beyond a wavelength of 2 μm, due to the onset of losses in silica, it is necessary to consider nonsilica "compound" glasses for the generation of broadband radiation. The fundamental material properties of these glasses can enhance supercontinuum generation across the mid-IR since these glasses can have intrinsic nonlinearities $\sim 10\times$ to $100\times$ that of silica. However, the ZDW of these materials are generally at longer wavelengths compared to silica, implying the need for longer wavelength pump lasers. The material dispersion is strongly dependent on the choice of glass, and one particularly attractive option is to use the unique waveguide dispersion characteristics of small-core MOF to shift the fiber zero-dispersion to below 2 μm to offer the potential of using diode-pumped solid-state lasers operating at wavelengths close to 2 μm to generate the supercontinuum. Seeding at 1.55 μm from an Er-fiber pump system is a very attractive option, and a zirconium barium lanthanide sodium fluoride (ZBLAN) fiber has been used to generate supercontinuum extending from 0.8–4.5 μm using 1.55-μm pumping [8]. Seed wavelengths of 2.0–2.25 μm are also readily accessible from commercially available OPO and optical parametric amplifier (OPA) systems as well as from Tm^{3+} and Ho^{3+} fiber sources.

High-nonlinearity compound glasses have not yet found widespread applications due to the difficulty in fabricating low-loss single-mode fibers. However, microstructured fiber technology provides a powerful new technique for producing compound glass structures, and fibers with tight mode confinement and tailored dispersion have already been demonstrated. For example, a compound glass microstructured fiber with loss of 3.5 dB/m and $\gamma = 1860/(\mathrm{W{\cdot}km})$ at 1550 nm was reported recently [9].

For many applications, a small fiber core is a desirable feature since the tight mode confinement provides high effective nonlinearity, and it enables tailoring of the ZDW to match the pump wavelength. Therefore, small-core fibers typically require low pulse energies to generate supercontinuum, which relaxes the source power requirements. However, for applications requiring high average powers, a small core limits the maximum pulse energies that can be used, and producing high average power necessitates vastly increasing the repetition rate of the source laser. In order to increase the pulse energy requirement to satisfy the average power needs for reasonable pulse repetition rates, it becomes necessary to work with fibers having a larger core area. In this instance, the dispersion of the fiber is dominated by the material dispersion, and it is not possible to shift the fiber ZDW to match the pump wavelength. Consequently, one can envisage

Manuscript received November 6, 2006; revised March 26, 2007. This work was supported in part by BAE Systems Virtual University (U.K.) and in part by SELEX Sensors and Airborne Systems (U.K.).

J. H. V. Price, F. Poletti, P. Horak, J. Y. Y. Leong, P. Petropoulos, J. C. Flanagan, G. Brambilla, X. Feng, and D. J. Richardson are with the Optoelectronics Research Centre, University of Southampton, Southampton SO17 1BJ, U.K. (e-mail: jhvp@orc.soton.ac.uk).

V. Finazzi is with the Institute of Photonic Sciences (ICFO), Barcelona 08860, Spain.

T. M. Monro and H. Ebendorff-Heidepriem are with the School of Chemistry and Physics, University of Adelaide, Adelaide SA 5371, Australia.

Digital Object Identifier 10.1109/JSTQE.2007.896648

a need for two sorts of fiber and two sorts of pump laser suited for either high- or low-power applications.

To assess the extent to which nonsilica MOF sources could be of benefit for mid-IR laser technology, a range of fiber parameters should be studied to provide an indication of what an optimized source could provide. In a previous conference paper, we presented the results of numerical simulations to indicate the optimum glass-type and fiber-design combinations for mid-IR supercontinuum generation when pumped at near-IR wavelengths by systematically varying each fiber parameter with other parameters held constant [10]. We established that for 200-fs near-IR seed pulses, the continuum was generated in <40-mm fiber lengths. We also showed that the dispersion was an important factor controlling the wavelength range of the continuum. Once the seed pulse energy was above a threshold level that is necessary for effective continuum generation, further increasing the energy or fiber nonlinearity led to only modest increases in the continuum bandwidth. However, in our previous study, we considered only seed wavelengths close to the fiber's lowest ZDW, which is the usual configuration for demonstrations of visible supercontinuum generation using Ti:sapphire [3] or rare-earth-doped fiber-pump lasers [11], [12]. As a consequence, although the tailored dispersion profiles of the small-core fibers did enable pumping at a shorter wavelength, we observed similar broadening in both small-core and large-modefibers.

Here, we have followed up our initial investigations of low-power sources based on a small-core Bi-based MOF fabricated by extrusion and have performed simulations for a range of small-core Bi MOFs with two ZDWs. The fibers have the same short-wavelength ZDW at 1.55 μm and long-wavelength ZDWs varying from 2.4 to 4.0 μm. The results show that enhanced mid-IR continuum broadening is possible using dispersion-tailored small-core fibers as compared to large-mode fibers. For comparison, we chose three nonsilica glasses as large-mode-area (LMA) fiber, which show the continuum produced from high pulse energy sources.

Based on the results of our review, we believe that nonsilica MOF technology is attractive for future practical sources. We show that using small-core MOFs with two ZDWs can enable efficient phase-matching from the <2-μm pump wavelength across the second ZDW into the mid-IR.

We expect that our mid-IR simulations should provide a reasonable guide to the spectra that might be possible from future experimental work, although they should not be considered exact predictions. Our numerical model is similar to that used by other authors for studying visible continuum in silica MOF [6]. In addition, we have previously published a study of visible/UV supercontinuum generation from a silica MOF [13] and a study of visible/near-IR supercontinuum from an extruded SF57 MOF [9]. Both of these studies combined experimental and numerical results, and the simulations and experiments were in qualitative agreement.

This paper is structured as follows. Section II presents an overview of the multicomponent glass properties and waveguide fabrication technologies as background for researchers unfamiliar with nonsilica glasses. Section III presents fiber designs that achieve a ZDW close to the pump wavelength chosen. Section IV presents the modeling predictions for the supercontinuum spectra. Section V contains our conclusions and suggestions about desirable fiber properties for future investigation.

II. Glass Choice and Fabrication Technologies

Supercontinuum generation at mid-IR wavelengths requires the use of a highly nonlinear optical medium with good mid-IR transparency. Extending current MOF technology developed from silica-based work at visible and near-IR wavelength ($\sim$0.4–1.7 μm) to mid-IR wavelengths (>2 μm) necessitates developing a detailed understanding of the relationship between the glass composition and the optical properties, such as the position of the multiphonon absorption edge and nonlinear refractive index, etc., in order to select a suitable glass for the fibers. We also consider multiple MOF fabrication approaches in order to tailor the dispersion and nonlinearity of thefibers.

The absorption of a solid in the long-wavelength limit is determined by what is known as the multiphonon or IR absorption edge, which arises from intermolecule or lattice vibrations. A simple Hooke's law mass-on-spring model predicts that the multiphonon absorption edge will shift toward longer wavelengths if heavier atoms are introduced into the glass network or if chemical bonds are weakened. The multiphonon absorption edges of several glasses are shown in Fig. 1(a) [14]. Note that due to the strong Si–O bonding, the oxide glasses containing SiO_2 cannot be transparent at wavelengths longer than 5 μm, and glasses containing any oxide cannot be transparent at wavelengths longer than $\sim$8 μm. We reviewed data on a variety of glass compositions and selected those with transmission loss due to multiphonon absorption of less than 2 dB/m at 2 μm for further consideration.

In addition to the phonon losses, extrinsic losses, which are due to scattering and impurity absorption can affect the glass transmission below the intrinsic maximum transmission wavelength. Oxide glasses readily incorporate OH impurities, which can result in losses of more than 1000 dB/m at certain wavelengths, as shown for Schott SF57 (lead oxide) glass and bismuth oxide glass in Fig. 1(b). Dehydration techniques such as the addition of fluoride and dry/reactive gas treatment can decrease the OH loss substantially. Fluoride glasses are generally less susceptible to OH impurities, and dehydration can then decrease the OH loss to as low as 0.001 dB/m [15]. In oxide glasses, the OH bands have very broad span over the whole mid-IR range, whereas the OH band of fluoride and chalcogenide glasses is confined to 2.8–3.4 μm. The OH and SH contents of chalcogenide glasses depend on the melting conditions, and with careful environmental control during fabrication, gallium lanthanum oxy-sulphide (GLSO) microstructured fiber has been produced at the University of Southampton with low OH absorption of 20 dB/m at 3 μm [Fig. 1(b)]. Commercial As_2S_3 fibers exhibit OH absorption of <2 dB/m at 3 μm and SH absorption of 2–10 dB/m at 4 μm.[1,2]

[1]http://www.amorphousmaterials.com
[2]http://www.coractive.com

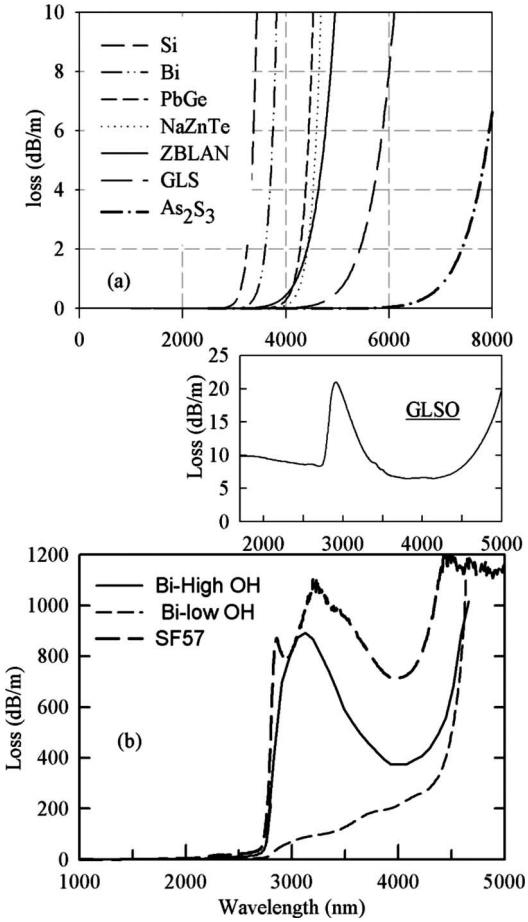

Fig. 1. (a) Multiphonon edge of different glasses (theoretical fit). (b) Loss spectra of Bismuth, SF57, and GLSO glasses (simulated) measured using meter lengths of unclad fiber and the cutback technique, or 1–30 mm thickness bulk glass samples, and a commercial spectrophotometer.

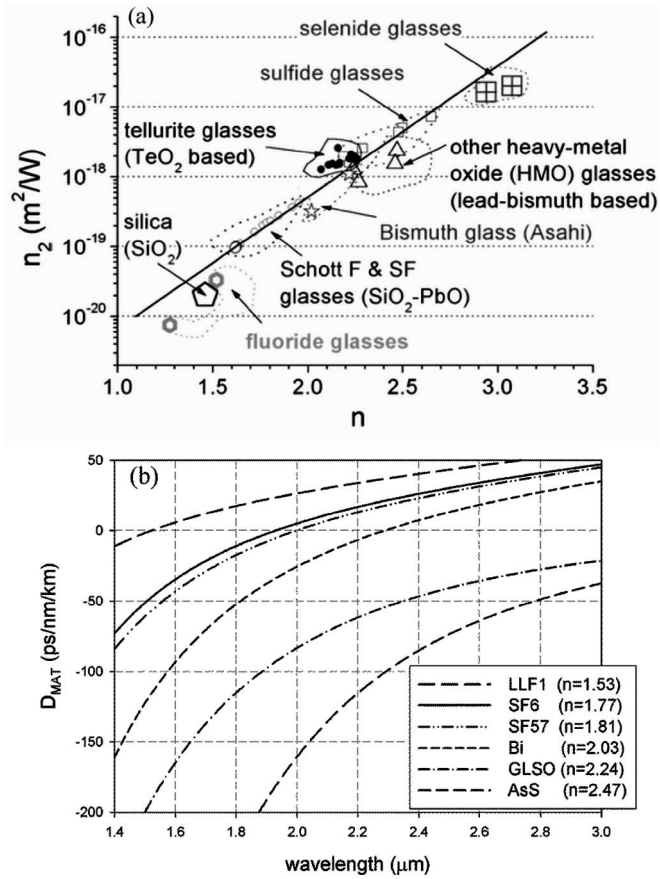

Fig. 2. (a) Relation between the linear refractive index n and nonlinear refractive index n_2 in various glasses. (b) Material dispersion curves of Schott glasses (LLF1, SF6, SF57), bismuth oxide glass (Bi), and chalcogenide glass (GLSO). The numbers in the legend indicate the linear index at 1.06 μm.

The small-core MOFs considered in this paper typically show waveguide losses of $\sim$2 dB/m (in addition to the material loss), due to scattering from core surface roughness and contaminants accumulated during fabrication. In addition, all modes of an MOF have an associated confinement loss (due to the finite extent of the cladding region) [16], but these losses can be reduced to low values by ensuring a sufficiently large microstructured cladding region. Therefore, the total fiber losses would be dominated by the rather high material losses, and with short lengths of fiber, considered in this paper, the waveguide-related losses can be considered to be negligible.

The refractive index and its variation with wavelength are also dependent on glass composition. In addition, a high-intrinsic nonlinearity is usually associated with a high linear refractive index according to the empirical Miller rule, which tells us that the third-order nonlinear dielectric susceptibility $\chi^{(3)}$ is proportional to the fourth power of the linear susceptibility $\chi^{(1)}$. A high nonlinear refractive index is expected to be achieved in glasses composed of ions with high polarizibility. However, we note that the Miller rule can only provide a rough indication of those materials with high values of n_2, and accurate values of n_2 must be obtained via experimental characterization. Fig. 2(a) shows a summary of the relation between the linear refractive index n and the nonlinear refractive index n_2 in various glasses [17]. It can be seen that introducing heavy atoms (i.e., heavy metal compounds) or ions with a large ionic radius (i.e., using chalcogen elements S, Se, and Te to replace oxygen) act to increase the polarizibility of the components in the glass matrix and also increase the nonlinear index n_2.

Supercontinuum generation depends on the fiber dispersion, not only at the pump wavelength, but also over a broad wavelength range. MOF structures that achieve a high degree of mode confinement enable a remarkable degree of dispersion management, but an inherently favorable material dispersion is still required if a broad, flat dispersion profile is to be obtained. To predict the refractive indices of the glasses at wavelengths above 2 μm we have used the measured refractive index data,[3,4] (see also footnote 1), fitted to a generalized Sellmeier equation. We have also calculated the material dispersion D_{MAT} for several glasses [Fig. 2(b)] from the Sellmeier equation fits. The linear and nonlinear indices, and the predicted ZDW ($D_{\mathrm{MAT}} = 0$) of different glasses are listed in Table I. The ZDW of a glass shifts to longer wavelength with increasing linear refractive index. Heavy metal oxide glasses (lead silicate, bismuth oxide,

[3]Data provided by Asahi Glass Company.
[4]http://www.schott.com

TABLE I
PROPERTIES OF DIFFERENT GLASSES

Glass type	code	Main components	n_0	$n_2 \times 10^{20}$ (m^2/W)	ZDW (μm)
silica	Si	SiO_2	1.45	2.7 [19]	1.26 [20]
lead silicate	SF57	$PbO\text{-}SiO_2$	1.81	41 [21]	2.00
bismuth oxide	Bi	Bi_2O_3	2.02	32 [22]	2.29
germanate	PbGe	$PbO\text{-}GeO_2$	1.80	22 [23]	1.78[b] [20]
Tellurite	ZnTe	$ZnO\text{-}TeO_2$	2.03	51 [19]	2.24[a] [20]
Fluoride	ZBLAN	$ZrF_4\text{-}BaF_2$	1.50	3.3 [19]	1.62 [15]
chalcogenide	AsS	As_2S_3	2.44	594 [24]	4.81
	GLS	$Ga_2S_3\text{-}La_2S_3$	2.41	216 [25]	
	GLSO	$Ga_2S_3\text{-}La_2O_3$	2.25	177 [25]	4.64

Linear and nonlinear indices n_0 and n_2 at 1.06 μm (Si, PbSi, PbGe, ZnTe, ZBLAN) and 1.5 μm (Bi, AsS, GLS, GLSO), and zero dispersion (ZDW).

[a] value for $Na_2O\text{-}TeO_2$ glass, [b] value for $Na_2O\text{-}GeO_2$ glass

tellurite) have linear indices in the range of 1.8–2.0, nonlinear indices $\sim$10 times higher than silica, material ZDWs of 2–3 μm, and multiphonon absorption edges at $\sim$3.5 μm. Chalcogenide glasses (GLS, As_2S_3) have linear indices of 2.2–2.4, nonlinear indices significantly greater than those of the oxide glasses, and ZDWs larger than 4 μm.

As a brief conclusion on the selection of the glass, we believe that heavy-metal-oxide- and chalcogenide-based glasses are promising candidates for developing mid-IR nonlinear MOFs. The chalcogenide glasses possess advantages in terms of higher n_2 and longer wavelength multiphonon absorption edges. However, although chalcogenide MOF technology is progressing rapidly [18], the fabrication technology for heavy-metal-oxide glass-based MOFs is perhaps more mature, and the heavy-metal-oxide-based glasses typically have lower toxicity and higher thermal stability compared to the chalcogenide-based glasses. In this paper, we have chosen to focus on a particular heavy metal oxide glass, and we devote particular attention to the tailored dispersion properties possible in small-core MOFs. When considering large-mode fibers, we have considered both heavy metal oxide and sulfide glasses in order to provide a range of dispersion profiles.

A review of fabrication technology is provided in order to establish an appropriate fiber geometry for the design optimization described in the following section. Three waveguide types can provide tight mode confinement to enable both dispersion management and high effective nonlinearity over extended interaction lengths: rib-waveguides, tapering of fibers, and MOFs. For fibers, and to a lesser extent tapers, the combination of loss and nonlinearity leads to scaling of device length to achieve an optimum nonlinear figure of merit [26]. Planar waveguides are longer than typical nonlinear crystal devices but shorter than fiber-based nonlinear devices. Therefore, for planar waveguides, high nonlinearity and dispersion tailoring are perhaps more critical than loss.

The thermomechanical properties of the glass are important for fabricating fibers, and compound glasses exhibit far lower processing temperatures than silica, (typical compound glass softening temperatures are $\sim$500 °C as opposed to $\sim$2000 °C for silica), which enables the use of extrusion for fiber preform manufacture [17]. In addition, the low processing temperature facilitates the use of ceramic microheaters for compound glass fiber tapering in contrast to CO_2 laser or flame burners used for silica taper fabrication [27].

Fiber tapering is an attractive option for nonsilica glasses since it enables postprocessing to fine-tune the dispersion characteristics without requiring new fibers to be drawn. For example, mid-IR continuum generation has been demonstrated using a bismuth fiber taper [27]. Using a silica MOF, tapering has also been used for dispersion micromanagement starting with a small-core fiber and then tapering to shift the ZDW to shorter wavelengths [28]. This technique enabled enhancement of spectral power generation in a variety of wavelength ranges and should also be applicable to nonsilica MOFs in the future.

The emergence of MOF fabrication technology is particularly enabling for multicomponent glasses as it eliminates the need for two thermally, chemically, and optically compatible glasses to form the fiber core and cladding as required for the conventional step-index fibers. MOF technology, thus, provides a simple and convenient route to realizing fibers in high-nonlinearity glasses that otherwise might not be able to be drawn into fiber form. Recent progress in extruded bismuth-oxide-based glasses has been particularly worth noting [29], and both lead silicate (Schott SF57 glass) [30], [31] and tellurite [32] MOFs have also been demonstrated. In addition, an As–Se MOF has been reported that generated IR supercontinuum extending from 2.1 to 3.2 μm using 2.5-μm pumping [33].

Several techniques have been used to fabricate compound glass MOFs [17]. One approach is to manually stack capillary tubes to produce the structured preform. This is the approach that is routinely used to produce silica microstructured fibers, and the resulting fibers typically consist of a hexagonal lattice of air holes surrounding the fiber core. It is anticipated that using the flexibility of this approach, fiber geometries could be designed to tailor the dispersion characteristics (for example, to achieve lower dispersion slope), but at present, this technique is not well developed for compound glasses.

A second fabrication approach that can be used for compound glasses (which in general have lower melting points than silica) is to use extrusion in producing the structured preform from bulk glass billets [34]. This technique has now been used to produce a broad range of fiber geometries in a number of compound glass materials including lead silicate [35], bismuth oxide [29], and tellurite [36] glass materials. The geometry that has been used for many of these demonstrations is the so-called "wagon-wheel" (WW) fiber, which is a micrometer-scale solid core suspended by three long fine glass struts that optically isolate the core within a robust solid jacket. A scanning electronic microscope (SEM) image of a WW fiber is shown in the inset to Fig. 3. In the WW fiber, the size of the core can be adjusted

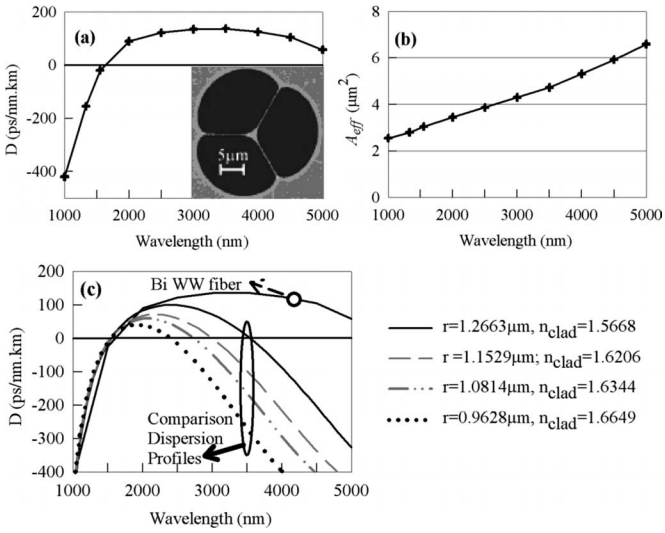

Fig. 3. (a) Dispersion for 2.6-μm core Bi glass WW fiber. The inset shows an SEM of a typical WW fiber. (b) Effective mode area (A_{eff}) for 2.6-μm core Bi glass WW fiber. (c) Dispersion profile of Bi glass WW fiber and of Bi glass circular rods (fiber cores) with variable radius and surrounding average refractive index as shown in the graph legend.

during the drawing process by modifying the outer fiber diameter. These fibers can readily be made with small cores and high numerical aperture (NA), leading to tight mode confinement, and thus, high fibernonlinearity.

Other demonstrated approaches for MOF fabrication with compound glasses include drilling the desired pattern of holes in the preform [17] and casting the structured preform [37], [38]. Drilling has the advantage of creating a multihole preform in one step, and achieves high dimensional-precision, but it suffers from somewhat poor surface quality and a low yield. Casting enables high dimensional-precision, and high air-filling fraction, but is suitable only with a limited choice of glasses.

III. Small-Core Microstructured Fiber Designs

This section describes our modeling of the optical properties possible in compound glass MOFs with the aim of identifying designs that are particularly suitable for supercontinuum generation. In this section, designs are considered for small-core fibers, for which the waveguide dispersion is large and can dominate the material dispersion. The aim of this section is to predict the dispersion and effective area of these fibers in sufficient detail to enable the modeling of supercontinuum generation.

Since LMA fibers have a rather small waveguide contribution to the dispersion, we have not considered a detailed review of LMA fiber designs. Possible LMA fiber structures include low air-fill MOF designs, as typically fabricated by capillary stacking, or the conventional step-index fibers based on two different glass compositions for the core and cladding.

Small-core high-NA MOF designs, in general, allow a broad range of dispersive properties to be achieved (depending on the detailed choice of the fiber geometry). The WW geometry has been used for initial investigation because, in addition to offering high nonlinearity, it is a geometry that has been demonstrated to be practical for fabrication and handling a range of glasses. The WW geometry also restricts the parameter space that needs to be investigated to a single parameter for each glass type (i.e., the core size). Our calculations used the orthogonal function technique [39], [40]. The advantages of this method are that it can accurately and efficiently scan a broad range of wavelengths and structures, the material dispersion can be included in the calculations *ab initio*, and it is an experimentally validated method for predicting the dispersion of real fiber structures from SEMs. We model the structure of a real fiber as taken from an SEM image of a typical WW fiber [see inset to Fig. 3(a)]. Note that all the results given here are for the fundamental mode, and our past experience indicates that 2–3 μm cores can be operated in an effectively single-mode fashion.

For these small-core WW fibers, we considered a pump wavelength of 1.55 μm, and we decided to focus on the example of Asahi bismuth oxide glass, which has been used extensively for the fabrication of high-quality WW fibers [29]. We performed a detailed calculation of the fiber dispersion to design a fiber with zero net dispersion at the 1.55-μm pump wavelength. The calculation included the full material dispersion (set using the fitted Sellmeier equation), and the required core diameter was 2.6 μm. (We note that others have suggested that using even smaller core sizes would be optimal when employing these fibers for visible continuum generation [41].) Fig. 3(a) and (b) shows the calculated net dispersion (D) and effective mode area (A_{eff}) [26] for this fiber at a discrete set of wavelengths: 1.0, 1.33, 1.55, 2.0, 2.5, 3.0, 3.5, 4.0, 4.5, and 5.0 μm. At 1.55 μm, the net dispersion is close to zero. The predicted fiber dispersion shows a very strong variation with wavelength due to the strong waveguide contribution, whereas A_{eff} is a more slowly varying function ofwavelength.

The shape of the dispersion curve across the mid-IR can have a strong influence on the wavelength span of the supercontinuum generation, as discussed in Section IV. It is well known that varying the core diameter and the effective cladding index for a silica MOF can lead to a wide variety of dispersion profiles [39]. To assess the sensitivity of the supercontinuum broadening to the changes in the dispersion profile, we also calculated the dispersion profiles for Bi-glass fibers based on an idealized structure in which the core of the fiber was approximated by a solid circular rod, and the cladding was taken to be a solid material with the average index of the microstructured cladding region. The advantage of the idealized structure is that the propagation constant can be calculated analytically [42]. (Similar dispersion profiles would be possible with real MOF structures fabricated using the stacking technique, as described in Section II.) The lower ZDW was maintained at 1.55 μm, and the dispersion profiles were predicted to have a second ZDW at longer wavelengths, as shown in Fig. 3(c). The choice of the dispersion design was in order to maintain a fixed relation between the pump wavelength and the lower ZDW. While other choices of flattened dispersion profile are possible, the designs chosen provided insight into the importance of the overall shape of the dispersion profile rather than variations in the relation of the pump and ZDW. Similar studies on the influence of dispersion variation in silica MOF for visible and near-IR continuum generation have been reported in [43], [44].

IV. Supercontinuum Simulations

To predict the supercontinuum spectra that could be obtained from each of the nonsilica MOFs considered, we performed numerical simulations. We have used the small-core Bi glass WW fiber (described in Section III) as a base case for our investigation, and we then studied how the continuum is affected by changes in the fiber loss and dispersion. For example, we compared large-mode fiber simulations including or excluding the fiber loss.

When seeding with ~200-fs pulses close to the fiber's ZDW, the initial pulse undergoes nonlinear compression, soliton fission, and then rapid spectral broadening over a typical "threshold length" of only a few centimetres [5]. The pulses then broaden temporally, causing a reduction of the peak power and the supercontinuum width saturates [45]. We have used a fiber length above this threshold length, and differences between spectra are, thus, attributed to different dispersion profiles, and not to length scales. In contrast to the results presented here, with longer duration seed pulses (e.g., >50 ps), the dominant mechanisms for spectral broadening are self-phase modulation (SPM) and four-wave mixing (FWM) [26], [46]. Therefore, a separate study would be required to predict the appropriate fiber lengths with much longer seed pulses and the possible output spectra.

The predicted spectra in all the graphs that follow are shown using a dBm/nm scale, assuming a pulse repetition rate of 1 Hz. This scale would show an average power of -30 dBm/nm for 1-μJ pulses with 1-nm spectral widths. Scaling the power spectra to different pulse repetition rates can be done as follows: e.g., starting with -90 dBm/nm at 1 Hz, and converting to 1 MHz (10^6 Hz) gives $(-90+60)=-30$ dBm/nm.

In this section, we first describe the numerical model used for the simulations in Section IV-A. Simulation results for various Bi glass small-core MOF dispersion designs are presented in Section IV-B. Section IV-C then shows simulations for large-mode fibers and also demonstrates the significance of loss.

A. Numerical Model

As with silica, we have assumed that the amorphous multicomponent glasses are centrosymmetric, and therefore, have no intrinsic second-order nonlinear susceptibility ($\chi^{(2)}$), and have a homogeneous third-order nonlinear susceptibility ($\chi^{(3)}$). The third-order nonlinear susceptibility is assumed to be small compared to the linear susceptibility, and is also assumed to be wavelength-independent over the wavelength range considered in this paper. The total refractive index, therefore, includes a small intensity-dependent nonlinear contribution ($n=n_0+n_2I$). Effects such as two-photon absorption have not been included. As noted in Section III, our experience is that 2–3 μm cores can be operated in an effectively single-mode fashion, and the low NA large-mode fibers that we consider could be rigorously single-mode structures throughout the mid-IR (i.e., above the pump wavelength). We have, therefore, considered only processes occurring within the fundamental fiber mode and not mode-mixing to possible higher order modes. These simplifications enable modeling of the pulse propagation using the modified nonlinear Schrödinger equation (NLSE) with loss [26], as follows:

$$\frac{\partial A}{\partial z}-i\sum_{k\geq 2}\frac{i^k\beta_k}{k!}\frac{\partial^k A}{\partial t^k}+\frac{\alpha(\omega)}{2}A = i\gamma\left(1+\frac{i}{\omega_0}\frac{\partial}{\partial t}\right)\left(A(z,t)\int_{-\infty}^{+t}R(t')|A(z,t-t')|^2dt'\right)$$

where $A(z,t)$ is the electric field envelope, ω_0 is the center frequency, $\gamma=(n_2\omega_0/cA_{\text{eff}})$, β_k are the dipersion coefficients at the center frequency, and $\alpha(\omega)$ is the frequency-dependent fiber loss. For the small-core WW fiber, we used the wavelength-dependent dispersion data from Fig. 3, and for the large-mode fibers, we ignored the smaller waveguide dispersion and used the bulk-glass dispersion from Fig. 2. We used the A_{eff} data from Section III as calculated at the seed pulse wavelength. To solve the propagation equation, we used a standard split-step Fourier algorithm treating dispersion in the frequency domain and the nonlinearity in the time domain, apart from the temporal derivative for the self-steepening effect, which was evaluated using Fourier transforms.

The model includes both the instantaneous electronic response (responsible for the Kerr effect), and the delayed ionic response (responsible for Raman scattering) in the nonlinear component of the refractive index n_2. As is usual when modeling silica fibers, the nonlinear response to the applied field $A(z,t)$ has been written as, $R(t)=(1-f_R)\delta(t)+f_Rh(t)$, where the δ-function represents the instantaneous electronic response, and $h(t)$ represents the delayed Raman response of the ions [26]. The modified NLSE has been used by other authors for the numerical study of supercontinuum generation [47], [48].

We are not aware of previous measurements of the delayed Raman responses of these multicomponent glasses. For silica, the Raman temporal response $h(t)$ has been previously determined from the shape of the Raman gain in the frequency domain [49], and $f_R=0.18$ was determined from measurements of the absolute value of the Raman gain. We calculated the shape of the delayed temporal responses of the multicomponent glasses from spontaneous Raman spectra measured by the authors, and using the procedure of Stolen *et al*. [50]. We have assumed that $f_R=0.2$, based on the known fraction of 0.18 for silica.

Due to our measurement setup, no spontaneous Raman data were available for the frequency range of 0–6 THz (0–200 cm^{-1}), and we have assumed a linear increase in the spontaneous Raman spectrum in this range. We believe this assumption is reasonable, particularly since the phonon data show a decreasing power at the lowest measured frequency. However, we note that 0–6 THz is an important frequency range because the frequency width [full-width at half-maximum (FWHM)] for a 200-fs transform-limited Gaussian pulse is 2.2 THz, and it is, therefore, this part of the Raman spectrum that provides the long wavelength gain for soliton self-frequency shifting (SSFS). In our previous study of multicomponent glass MOFs, we showed the spectra from simulations performed for Bi glass WW fiber for the same seed pulse parameters and with: 1) SPM term only; 2) SPM and self-steepening terms; and 3) including the Raman response [10]. The overall shape of the continuum was similar in all cases, and we concluded that the initial continuum

generation is not highly dependent on the Raman response in the fiber. Therefore, although the exact form of the Raman response is uncertain for these glasses, small differences should lead to only small changes in our predicted spectra.

We note that there are further refinements that can be made to the aforementioned NLSE to include effects, such as polarization coupling and the wavelength dependence of A_{eff}, but the simulations as they stand should provide a reasonable estimate of the expected spectra. Our simulation results show the expected fine structuring [47], and we have applied a rolling average to smooth the spectra. These smoothed spectra should be approximately comparable to the time average over several pulses that would be measured in experiments where the seed pulses have small energy fluctuations. The simulated seed pulse was taken to have a transform-limited Gaussian profile at the relevant center wavelength.

B. Simulations Demonstrating the Significance of Dispersion in Small-Core Bi MOF

For the reference example of the small-core Bi glass WW fiber, as described in Section III, we first show simulations with various combinations of seed wavelengths and dispersion profiles. All of our small-core Bi MOF simulations include the loss profile of the Bi low-OH fiber, as shown in Fig. 1(b). In the small-core Bi MOF simulations, we fixed the pulse energy at 1 nJ, $T_0 = 0.2$ ps (FWHM), and fiber length to be equal to 40 mm, as this combination was found to be suitable for demonstrating supercontinuum in our earlier study [10]. As described in Section IV-C, for the large-mode fiber simulations, the seed pulse energy was increased to 30 nJ.

Our results are presented in the following order. We first use a seed wavelength equal to short wavelength ZDW at 1.55 μm with the full range of the fiber dispersion profiles. Then, we investigate a single dispersion profile with seed wavelengths ranging between the short- and long-wavelength ZDWs. We then return to the full range of comparison dispersion profiles and considered a seed wavelength approximately midway between the two ZDWs.

The spectra that result using a 1.55-μm seed wavelength are shown in Fig. 4. For the Bi WW fiber, the supercontinuum extended only to $\lambda = 2.2$ μm, which led us to consider fibers with a wider range of dispersion profiles, as shown in Fig. 4(a). For the dispersion profiles with closely spaced ZDWs, the spectra broaden to 3.0–3.5 μm by phase-matching to wavelengths above the second ZDW where the dispersion is normal. We concluded that the dispersion profile of the small-core Bi glass WW fiber was limiting the supercontinuum broadening to $\sim$2.2 μm and that MOF designs with two ZDWs were interesting for further consideration. At the shorter wavelength edge of the continuum, there is minimal variation between fibers, which is probably due to the steep dispersion profiles that naturally result from the tight mode confinement required to create the appropriate waveguide dispersion needed to compensate the bulk material ZDW of >2 μm and provide an overall fiber ZDW at the Er-pump wavelength of $\sim$1.55 μm.

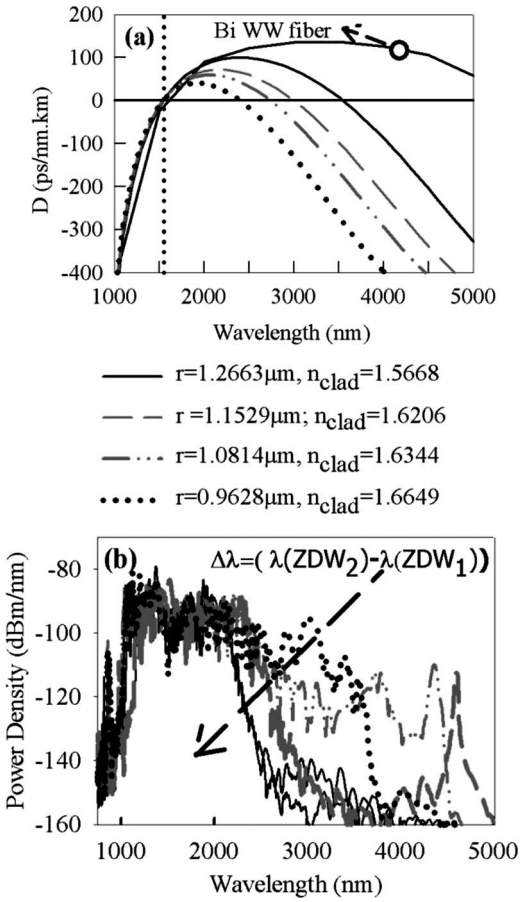

Fig. 4. (a) Dispersion profile of Bi glass WW fiber and of Bi glass circular rods (fiber cores) with variable radius and surrounding average refractive index as shown in the graph legend. The pump wavelength is at the lower ZDW ($\lambda_{\text{seed}} = 1.55$ μm). (b) Spectra for Bi glass MOF using the dispersion profiles shown in (a). [$E_0 = 1$ nJ, $T_0 = 0.2$ ps, fiber length $= 40$ mm, loss: low-OH Bi glass shown in Fig. 1(b)].

We also considered variation of the seed wavelength between the lower and upper ZDW in order to establish the optimum relation of the seed wavelength to the short- and long-wavelength ZDWs. We selected seed wavelengths of 1.55, 2.0, 2.5, and 3.0 μm, and used the dispersion profile with $r_{\text{core}} = 1.2663$ μm that has upper ZDW at $\sim$3 μm (see legend in Fig. 4 for the index of fiber cladding). Fig. 5(a) and (b) shows that seed wavelengths of 1.55 and 3 μm, which are close to the lower and upper ZDWs, respectively, each produced continuum spectra close to the related ZDW but not extending past the more distant ZDW. However, seed wavelengths of 2.0 and 2.5 μm, which are approximately midway between the ZDWs, produced much broader continuum spectra which extended across both ZDWs, as shown in Fig. 5(c) and (d). We concluded that a seed wavelength approximately midway between the ZDWs enabled the broadest spectra to be produced.

Next, we investigated spectra resulting from the range of circular rod dispersion profiles when using a seed wavelength of 2.0 μm, which is between the ZDWs. The resulting spectra are shown in Fig. 6. The position of the upper ZDW has clearly influenced the extent of the mid-IR continuum. In the fiber with upper ZDW at $\sim$4 μm, where the seed wavelength is closer to

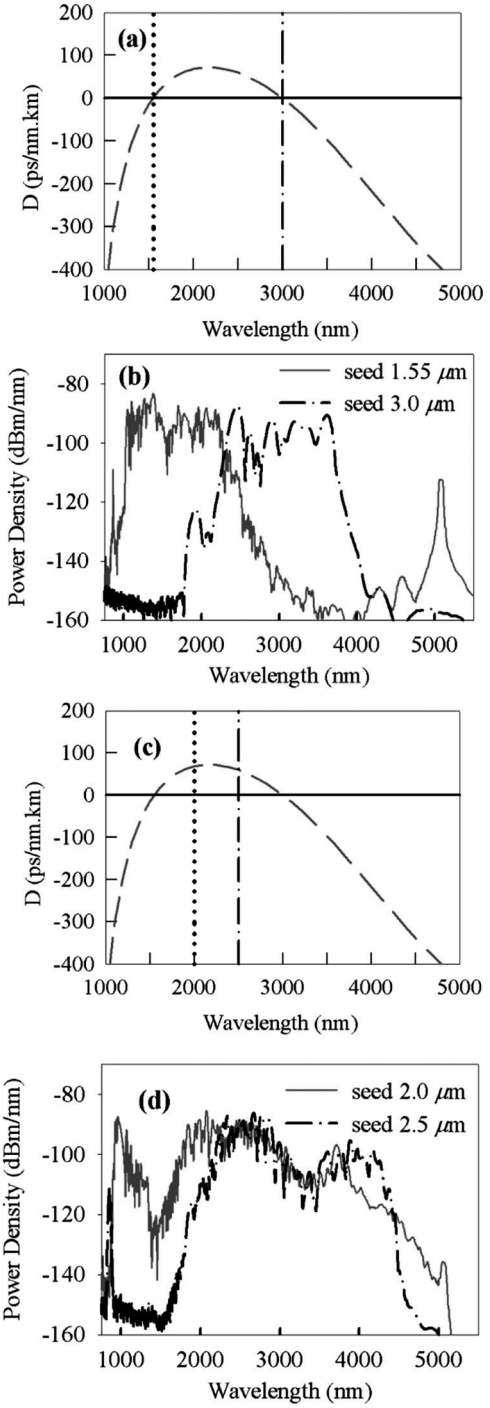

Fig. 5. Spectra for Bi glass circular fiber with core radius $= 1.2663\,\mu$m. Vertical lines show seed wavelengths. (a), (b) Seed wavelengths close to ZDWs: $\lambda_{\text{seed}} = 1.55\ \mu$m, $3.0\ \mu$m. (c), (d) Seed wavelengths between ZDWs: $\lambda_{\text{seed}} = 2.0, 2.5\ \mu$m. (Fiber length $= 40$ mm, loss: low-OH Bi glass shown in Fig. 1(b), $E_0 = 1$ nJ, $T_0 = 0.2$ ps.)

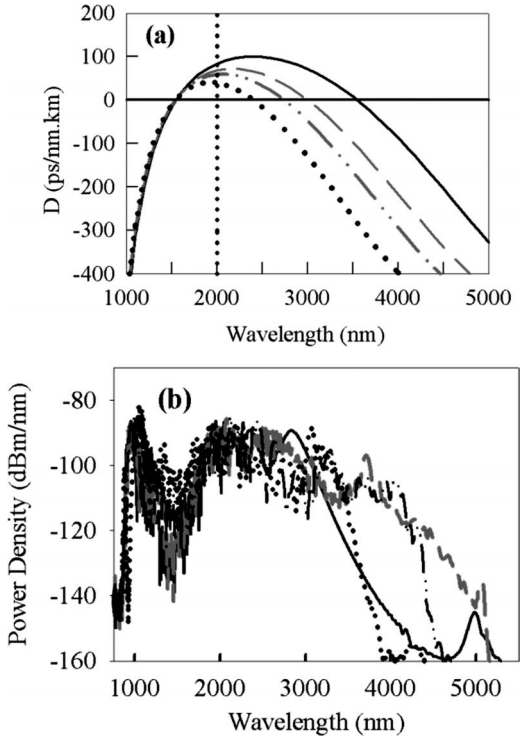

Fig. 6. Spectra for small-core Bi glass circular fibers with various dispersion profiles (see legend in Fig. 4. for core radii and cladding index). The seed wavelength is midway between the fiber ZDWs: $\lambda_{\text{seed}} = 2.0\ \mu$m [shown by dotted line in (a)]. (a) Dispersion profiles. (b) Continuum spectra. Line styles show corresponding spectra and dispersion profiles. (Fiber length $= 40$ mm, loss: low-OH Bi glass shown in Fig. 1(b), $E_0 = 1$ nJ, $T_0 = 0.2$ ps.)

the lower ZDW than to the upper ZDW, the broadening is mainly due to SSFS [51]. In contrast with the upper ZDW at $\sim 3\ \mu$m, there is phase-matched power transfer across that ZDW to the 4–5 μm range.

As the pulses propagate along the fiber in the anomalous dispersion region, they form solitons, which in turn generate dispersive waves in the normal dispersion region and lead to broad continuum generation. The wavelength of these dispersive waves is determined by a phase-matching condition [4], and we have calculated the phase-matched wavelengths, as shown in Fig. 7. In considering the nonlinear term in the phase-matching equation, we have assumed that the seed pulse initially generates a high-order soliton, which subsequently decays into fundamental solitons because of higher order dispersion. The most powerful of the fundamental solitons has a peak power of $P_0(2N_{\text{sol}} - 1)^2/N_{\text{sol}}^2$, where P_0 is the peak power of the input pulse, and N_{sol} is the soliton order corresponding to the input pulse. The peak power of the most powerful fundamental soliton is used for the nonlinear term since it is this soliton that is mainly responsible for the generation of dispersive waves. During the process of generating dispersive waves, the soliton experiences a recoil effect, which guarantees energy conservation. Because of the two ZDWs for the fibers considered here, dispersive waves can be amplified at shorter and longer wavelengths than the pump to transfer energy in a single step into the mid-IR.

To explain the supercontinuum spectra from the simulations, we note that although Fig. 7 shows phase-matching to long wavelengths is possible with solitons initially close to the lower ZDW, power transfer also requires that the soliton overlap spectrally with the dispersive wave. When seeding close to a ZDW, the soliton formed in the anomalous dispersion window

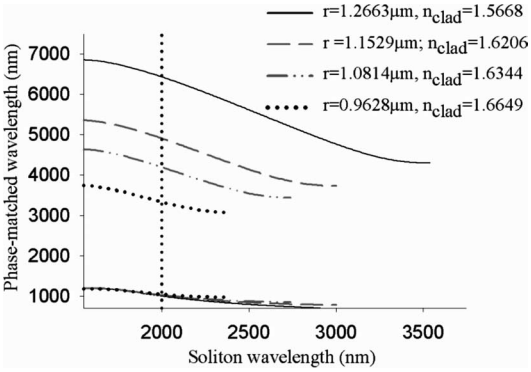

Fig. 7. Soliton phase-matching wavelengths for Bi glass circular fibers. The vertical line shows $\lambda_{\text{seed}} = 2.0$ μm. ($E_0 = 1$ nJ, $T_0 = 0.2$ ps; see text for parameters of the highest energy soliton fission pulse for these seed pulses.)

(between the ZDWs) may not have wings extending as far as the second ZDW, and in that case, no power is transferred beyond the second ZDW. In contrast, a broad soliton initially midway between the ZDWs could efficiently transfer power across both ZDWs.

In an experiment, the maximum pulse energy will be limited either by the available pump laser or by the material damage threshold. Input facet damage has been reported when launching pulses with similar duration and energy to those considered in this study when using small-core silica MOF for visible/UV supercontinuum experiments [13], [52] (although the precise damage mechanism was not identified). We might, therefore, expect that in experiments, fiber facet damage may occur for multicomponent glass MOF, but at present, we have no detailed data on damage thresholds for the particular glasses considered. In future, small-core fibers could perhaps be used to optimize the dispersion profile in order to minimize the required pulse energy.

We concluded that small-core MOFs with two ZDWs can enable greatly enhanced efficiency of mid-IR continuum from convenient pump wavelengths by phase-matching across the upper ZDW. This is a unique property available with MOF technology since it requires tighter mode confinement than is available with the conventional fibers. The appropriate pump wavelength would appear to be between the ZDWs and slightly toward the upper ZDW to promote power transfer to longer wavelengths as opposed to shorter wavelengths.

C. High-Power Mid-IR Continuum Using Large-Mode Fibers

In order to increase the pulse energy, it becomes necessary to work with fibers having a larger core area in order to avoid material damage. Since the LMA fiber dispersion is almost equal to the material dispersion, changing dispersion profile for a given pump wavelength requires the use of a different glass, which would also have different intrinsic nonlinearity. We, therefore, considered Bi, SF57, and GLSO glasses to demonstrate the range of spectra possible from LMA fibers.

In selecting an appropriate mode area for simulations, we observed that for silica MOF, the largest single-mode fiber available has $A_{\text{eff}} \sim 1000$ μm^2 (Crystal Fiber A/S DC-170-40-Yb). Nonsilica glasses have larger refractive indices compared to silica and are more challenging to fabricate. Therefore, as a reference case, we simulated the supercontinuum for an $A_{\text{eff}} \sim 100$ μm^2 fiber. (This A_{eff} does not correspond to a particular design, but is representative of what might be suitable for a low-NA fiber, providing approximately single-mode operation [53].) The 100-μm^2 mode area is $\sim$30 times greater than that for the small-core Bi glass fiber considered earlier, and the LMA fiber has correspondingly reduced effective nonlinearity. We used the same seed pulse duration of 0.2 ps as that for the small-core simulations, and we maintained approximately the same initial peak intensity by scaling the pulse energy by the ratio of the mode areas: (100 μm^2/3.05 μm^2) $\times$ 1 nJ $\approx$ 30 nJ. The chosen seed wavelength was 2.25 μm, which is close to the ZDW of Bi glass.

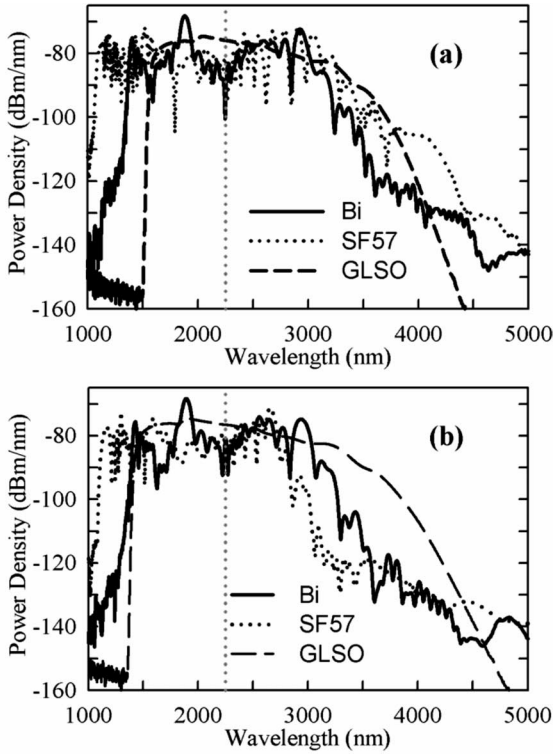

Fig. 8. Supercontinuum spectra predicted for LMA fibers of Bi, SF57, and GLSO glasses. (a) Excluding loss and (b) including losses shown in Fig. 1(b) (low-OH Bi glass chosen). (Fiber length = 40 mm, $T_0 = 0.2$ ps, $E_0 = 30$ nJ, $\lambda_{\text{seed}} = 2.25$ μm shown by dotted vertical line.)

The supercontinuum spectra, as shown in Fig. 8(a), were obtained with the loss set to zero, and for comparison, the spectra, as shown in Fig. 8(b), include the losses from Fig. 1(b) (low-OH Bi glass chosen). The spectra without loss for Bi and SF57 glasses extend to $\sim$3.5 μm. The seed wavelength is close to the ZDW of Bi glass and slightly above the ZDW of SF57 glass [see Fig. 2(b)]. Although the dispersion profiles of these glasses are less steep compared to that of the Bi WW MOF, we suggest that the dispersion slope again prevents more extended broadening. When loss is included [Fig. 8(b)], the low-OH Bi spectrum is only slightly attenuated between $\sim$3–3.5 μm but the SF57 spectrum is strongly attenuated at these wavelengths. By comparing the integrated output power of the simulations with and without loss, we calculated that for the dehydrated Bi fiber,

approximately 5% of the power was absorbed due to losses, whereas for the nondehydrated SF57 fiber, approximately 30% of the power was absorbed due to losses. Such high losses due to the OH absorption peak could lead to thermal issues; so, it could be important to use dehydrated glass samples when considering oxide glasses for high average power mid-IR sources. Multiphonon losses rise rapidly to very high levels at wavelengths close to ~ 5 μm, so high losses will again dominate the spectra if longer seed wavelengths enabled the supercontinuum from oxide glasses to extend to these wavelengths.

The supercontinuum spectrum of the GLSO fiber extends to ~ 3.8 μm. The seed wavelength is significantly below the ZDW of GLSO, so the dispersion of GLSO fiber in the continuum wavelength range is normal. The smooth continuum is, therefore, due to pure SPM broadening, as opposed to the soliton fission process. This spectrum would, thus, have good temporal coherence for pulse compression or metrology applications. In addition, the spectral broadening in this fiber would be expected to increase steadily with the initial pulse peak power. This is different from our findings for anomalously dispersive fibers in which continuum broadening saturates above a given seed pulse energy. Pumping large-mode GLSO fiber at longer wavelengths that are closer to the ZDW should, thus, produce broader spectra.

These results show that nonsilica LMA fibers are promising candidates for high-power mid-IR sources. Although the dispersion profile and seed wavelength are more favorable for Bi and SF57 glasses, the much higher nonlinearity of GLSO glass results in a similar broadening of the continuum at long wavelengths for all the fibers. The highest nonlinearity sulfide glasses are, therefore, likely to produce the broadest spectra when using pump wavelengths > 2.5 μm. As expected, we find that due to the larger mode area, higher pulse energies are required compared to small-core MOFs. The material dispersion dominates over the much smaller waveguide contribution in these larger scale structures, so, dispersion tailoring to match the convenient pump sources is not possible in LMA fibers, and thus, they require longer pump wavelengths.

V. Conclusion

We have considered whether the latest developments in nonsilica MOF technology could lead to practical mid-IR continuum sources from 2 to 5 μm. The optical properties of nonsilica glasses include a broad mid-IR transmission window and significantly higher intrinsic nonlinearities compared to silica. Microstructured fiber technology is enabling for many of these glasses since they can be hard to fabricate using the conventional fiber technology due to thermal stresses between mismatched core and cladding glasses. In addition, the low softening temperatures of multicomponent glasses enable extrusion to be used for efficient fiber fabrication. A unique property of MOFs is that high core/cladding index contrast can provide tight mode confinement for dispersion tailoring.

Results from numerical simulations indicate that with pump pulses of 0.2-ps duration, 1-nJ energy, and 2.0-μm wavelength, small-core fiber designs produced mid-IR continuum extending to 4.5 μm. LMA fibers suitable for higher pulse energies produced mid-IR continuum extending to 3.5 μm with pump pulses of 0.2-ps duration, 30-nJ energy, and 2.25-μm seed wavelength.

For small-core MOFs, we have demonstrated the advantage of dispersion-tailored small-core fibers in which the upper of two ZDWs can be used to phase-match near-IR pump wavelengths into the mid-IR. This has a further practical advantage since the material damage thresholds of these glasses are not yet well understood, and MOF designs that reduce the threshold peak intensity required for continuum generation could, therefore, be important. Based on these encouraging results, we suggest that a future study considering the effects of varying the dispersion profile might also encompass dispersion-flattened designs enabled by MOFs.

We also investigated continuum generation in large-mode fibers. For these fibers, the dispersion is close to that of the bulk material, and changing the dispersion requires switching the choice of glass. Since the material dispersion of many nonsilica glasses is high and normal at wavelengths below 2 μm, these fibers appear to have unfavorable dispersion properties for pumping in the 1.55–1.9 μm wavelength range. However, for pump wavelengths of 2.0–2.5 μm, LMA fibers made from oxide glasses have a well-matched material dispersion profile and should produce continuum extending to approximately 3.5 μm. In addition, although the ZDW of the high-nonlinearity sulfide glasses is above 3 μm, simulations show that such fibers produce similar continuum broadening and would have high-temporal coherence as it is generated in the normal dispersion region.

The fiber lengths required for generating continuum are < 40 mm, so, the losses of the fibers do not appear to dominate the spectra at wavelengths below ~ 4.5 μm provided that dehydrated glasses are used. However, losses due to the OH absorption peak could lead to thermal issues, so it is important to use dehydrated glass samples when considering oxide glasses for high average power mid-IR sources. If the supercontinuum spectra extend to ~ 4.5 μm, then high multiphonon losses can again dominate the spectra of the oxide glasses even for these short fiber lengths.

In conclusion, based on our results using fiber parameters available from demonstrated fiber technology and with readily obtainable seed pulse energies, we suggest that efficient mid-IR supercontinuum sources should be possible in the near future based on nonsilica MOF technology. The dispersion tailoring in small-core fibers is a clear advantage when comparing with the continuum generation in the LMA fibers since small-core fibers enable both the use of shorter wavelength pump lasers, and can produce broader mid-IR continuum. Compared to planar ribwaveguides or fiber-tapers, MOF technology has the advantages of greater flexibility for tailoring the dispersion profile over a broad wavelength range and a much wider possible range of device lengths.

Acknowledgment

The authors would like to thank R. Paschotta of RP Photonics Consulting (www.rp-photonics.com) for providing the ProPulse software for pulse propagation modeling. They would also like to thank Prof. D. Hewak and Dr. A. Favre for the helpful discussions.

REFERENCES

[1] R. Holzwarth, T. Udem, T. W. Hansch, J. C. Knight, W. J. Wadsworth, and P. S. J. Russell, "Optical frequency synthesizer for precision spectroscopy," *Phys. Rev. Lett.*, vol. 85, pp. 2264–2267, 2000.

[2] I. Hartl, X. D. Li, C. Chudoba, R. K. Ghanta, T. H. Ko, J. G. Fujimoto, J. K. Ranka, and R. S. Windeler, "Ultrahigh-resolution optical coherence tomography using continuum generation in an air-silica microstructure optical fiber," *Opt. Lett.*, vol. 26, pp. 608–610, 2001.

[3] J. K. Ranka, R. S. Windeler, and A. J. Stentz, "Visible continuum generation in air-silica microstructure optical fibers with anomalous dispersion at 800 nm," *Opt. Lett.*, vol. 25, pp. 25–27, 2000.

[4] A. V. Husakou and J. Herrmann, "Supercontinuum generation of higher-order solitons by fission in photonic crystal fibers," *Phys. Rev. Lett.*, vol. 87, pp. 203901-1–203901-4, 2001.

[5] J. Herrmann, U. Griebner, N. Zhavoronkov, A. Husakou, D. Nickel, J. C. Knight, W. J. Wadsworth, P. St.J Russell, and G. Korn, "Experimental evidence for supercontinuum generation by fission of higher-order solitons in photonic fibers," *Phys. Rev. Lett.*, vol. 88, pp. 173901-1–173901-4, 2002.

[6] J. M. Dudley, G. Genty, and S. Coen, "Supercontinuum generation in photonic crystal fiber," *Rev. Mod. Phys.*, vol. 78, p. 1135, 2006.

[7] P. Petropoulos, T. M. Monro, W. Belardi, K. Furusawa, J. H. Lee, and D. J. Richardson, "2R-regenerative all-optical switch based on a highly nonlinear holey fiber," *Opt. Lett.*, vol. 26, pp. 1233–1235, 2001.

[8] C. Xia, M. Kumar, M.-Y. Cheng, O. P. Kulkarni, V. Alexander, M. Islam, A. Galvanauskas, F. L. Terry, M. J. Freeman, M. Polulain, and G. Mazé, "0.8–4.5 microns supercontinuum generation in ZBLAN fluoride fibers scaled up to 1.25 W power," presented at the Conf. Lasers Electro-Opt., Longbeach, CA, 2006, Postdeadline paper CPDA10.

[9] J. Y. Y. Leong, P. Petropoulos, J. H. V. Price, H. Ebendorff Heidepriem, S. Asimakis, R. C. Moore, K. E. Frampton, V. Finazzi, X. Feng, T. M. Monro, and D. J. Richardson, "High-nonlinearity, dispersion-shifted lead-silicate holey fibers for efficient 1-μm pumped supercontinuum generation," *J. Lightw. Technol.*, vol. 24, no. 1, pp. 183–190, Jan. 2006.

[10] J. H. V. Price, T. M. Monro, H. Ebendorff Heidepriem, F. Poletti, V. Finazzi, J. Y. Y. Leong, P. Petropoulos, J. C. Flanagan, G. Brambilla, X. Feng, and D. J. Richardson, "Non-silica microstructured optical fibers for mid-IR supercontinuum generation from 2 μm–5 μm (Invited Paper)," in *Proc. SPIE, Fiber Lasers III: Technology, Systems, Applications,* vol. 6102, A. J. W. Brown, J. Nilsson, D. J. Harter, and A. Tünnermann, Eds. Bellingham, WA: SPIE, 2006, p. 61020A.

[11] J. H. V. Price, W. Belardi, T. M. Monro, A. Malinowski, A. Piper, and D. J. Richardson, "Soliton transmission and supercontinuum generation in holey fiber, using a diode pumped ytterbium fiber source," *Opt. Exp.*, vol. 10, pp. 382–387, 2002.

[12] H. Hundertmark, D. Kracht, D. Wandt, C. Fallnich, V. Kumar, A. K. George, J. C. Knight, and P. S. Russell, "Supercontinuum generation with 200 pJ laser pulses in an extruded SF6 fiber at 1560 nm," *Opt. Exp.*, vol. 11, pp. 3196–3201, 2003.

[13] J. H. Price, T. M. Monro, K. Furusawa, W. Belardi, J. C. Baggett, S. J. Coyle, C. Netti, J. J. Baumberg, R. Paschotta, and D. J. Richardson, "UV generation in a pure silica holey fiber," *Appl. Phys. B—Lasers Opt.*, vol. 77, pp. 291–298, 2003.

[14] D. J. Brady, T. Schweizer, J. Wang, and D. W. Hewak, "Minimum loss predictions and measurements in gallium lanthanum sulphide based glasses and fibre," *J. Non-Cryst. Solids*, vol. 242, pp. 92–98, 1998.

[15] P. W. France, S. F. Carter, M. W. Moore, and C. R. Day, "Progress in fluoride fibres for optical communications," *Brit. Telecommun. Technol. J.*, vol. 5, pp. 28–44, 1987.

[16] T. P. White, R. C. McPhedran, C. M. de Sterke, L. C. Botten, and M. J. Steel, "Confinement losses in microstructured optical fibers," *Opt. Lett.*, vol. 26, pp. 1660–1662, 2001.

[17] X. Feng, A. K. Mairaj, D. W. Hewak, and T. M. Monro, "Nonsilica glasses for holey fibers," *J. Lightw. Technol.*, vol. 23, no. 6, pp. 2046–2054, Jun. 2005.

[18] F. Smektala, L. Brilland, T. Chartier, T. N. Nguyen, N. Traynor, and T. Jouan, "Recent advances in the development of holey optical fibres based on sulphide glasses," presented at the SPIE Photon. West Conf., San Jose, CA, Jan. 2006, Paper 6128–19.

[19] E. M. Vogel, M. J. Weber, and D. M. Krol, "Nonlinear optical phenomena in glass," *Phys. Chem. Glasses*, vol. 32, pp. 231–254, 1991.

[20] S. Fujino and K. Morinaga, "Material dispersion and its compositional parameter of oxide glasses," *J. Non-Cryst. Solids*, vol. 222, pp. 316–320, 1997.

[21] S. R. Friberg and P. W. Smith, "Nonlinear optical-glasses for ultrafast optical switches," *IEEE J. Quantum Electron.*, vol. 23, no. 12, pp. 2089–2094, Dec. 1987.

[22] K. Kikuchi, K. Taira, and N. Sugimoto, "Highly nonlinear bismuth oxide-based glass fibres for all- optical signal processing," *Electron. Lett.*, vol. 38, pp. 166–167, 2002.

[23] D. W. Hall, M. A. Newhouse, N. F. Borrelli, W. H. Dumbaugh, and D. L. Weidman, "Nonlinear optical susceptibilities of high-index glasses," *Appl. Phys. Lett.*, vol. 54, pp. 1293–1295, 1989.

[24] J. M. Harbold, F. O. Ilday, F. W. Wise, J. S. Sanghera, V. Q. Nguyen, L. B. Shaw, and I. D. Aggarwal, "Highly nonlinear As-S-Se glasses for all-optical switching," *Opt. Lett.*, vol. 27, pp. 119–121, 2002.

[25] J. Requejo Isidro, A. K. Mairaj, V. Pruneri, D. W. Hewak, M. C. Netti, and J. J. Baumberg, "Self refractive non-linearities in chalcogenide based glasses," *J. Non-Cryst. Solids*, vol. 317, pp. 241–246, 2003.

[26] G. P. Agrawal, *Nonlinear Fiber Optics*, 2nd ed. San Diego, CA: Academic, 1995.

[27] G. Brambilla, F. Koizumi, V. Finazzi, and D. J. Richardson, "Supercontinuum generation in tapered bismuth silicate fibres," *Electron. Lett.*, vol. 41, pp. 795–797, 2005.

[28] F. Lu, Y. J. Deng, and W. H. Knox, "Generation of broadband femtosecond visible pulses in dispersion-micromanaged holey fibers," *Opt. Lett.*, vol. 30, pp. 1566–1568, 2005.

[29] H. Ebendorff Heidepriem, P. Petropoulos, S. Asimakis, V. Finazzi, R. C. Moore, K. Frampton, F. Koizumi, D. J. Richardson, and T. M. Monro, "Bismuth glass holey fibers with high nonlinearity," *Opt. Exp.*, vol. 12, pp. 5082–5087, 2004.

[30] J. Y. Y. Leong, P. Petropoulos, S. Asimakis, H. Ebendorff Heidepriem, R. C. Moore, K. Frampton, V. Finazzi, X. Feng, J. H. V. Price, T. M. Monro, and D. J. Richardson, "A lead silicate holey fiber with $\gamma = 1860\ \mathrm{W}^{-1}\ \mathrm{km}^{-1}$ at 1550 nm," presented at the Opt. Fiber Commun. Conf. (OFC), Los Angeles, CA, 2005, Paper PDP22.

[31] J. Y. Y. Leong, S. Asimakis, F. Poletti, P. Petropoulos, X. Feng, R. C. Moore, K. E. Frampton, T. M. Monro, H. Ebendorff Heidepriem, W. H. Loh, and D. J. Richardson, "Towards zero dispersion highly nonlinear lead silicate glass holey fibres at 1550 nm by structured-element-stacking," presented at the 31st Eur. Conf. Opt. Commun., Glasgow, U.K., 2005, Postdeadline paper TH.4.4.5.

[32] T. Delmonte, M. A. Watson, E. J. O Driscoll, T. M. Monro, V. Finazzi, P. Petropoulos, J. H. V. Price, W. Loh, X. Feng, J. C. Baggett, D. J. Richardson, and D. P. Hand, "Generation of mid-IR continuum using tellurite microstructured fiber," presented at the Conf. Lasers Electro-Opt., Longbeach, CA, 2006, Paper CTuA4.

[33] L. B. Shaw, P. A. Thielen, F. H. Kung, V. Q. Nguyen, J. S. Sanghera, and I. D. Aggarwal, "IR supercontinuum generation in As-Se photonic crystal fiber," presented at the Conf. Adv. Solid State Lasers (ASSL), Seattle, WA, 2005, Paper TuC5.

[34] T. M. Monro, "Progress in non-silica microstructured fibres," presented at the SPIE Photon. West Conf., San Jose, CA, 2006, Paper 6116-01.

[35] P. Petropoulos, H. Ebendorff-Heidepriem, V. Finazzi, R. C. Moore, K. Frampton, D. J. Richardson, and T. M. Monro, "Highly nonlinear and anomalously dispersive lead silicate glass holey fibers," *Opt. Exp.*, vol. 11, pp. 3568–3573, 2003.

[36] X. Feng, T. M. Monro, V. Finazzi, R. C. Moore, K. Frampton, P. Petropoulos, and D. J. Richardson, "Extruded singlemode, high-nonlinearity, tellurite glass holey fiber," *Electron. Lett.*, vol. 41, pp. 835–837, 2005.

[37] A. Mori, K. Shikano, W. Enbutsu, K. Oikawa, K. Naganuma, M. Kato, and S. Aozasa, "15 μm band zero-dispersion shifted tellurite photonic crystal fibre with a nonlinear coefficient γ of 675 $\mathrm{W}^{-1}\mathrm{km}^{-1}$," presented at the Eur. Conf. Opt. Commun. (ECOC), Stockholm, Sweden, 2004, Paper Th3.3.6.

[38] Z. Guiyao, H. Zhiyun, L. Shuguang, and H. Lantian, "Fabrication of glass photonic crystal fibres with die-cast process," *Appl. Opt.*, vol. 45, pp. 4433–4436, 2006.

[39] T. M. Monro, D. J. Richardson, N. G. R. Broderick, and P. J. Bennett, "Holey optical fibers: An efficient modal model," *J. Lightw. Technol.*, vol. 17, no. 6, pp. 1093–1102, Jun. 1999.

[40] T. M. Monro, N. G. Broderick, and D. J. Richardson, "Exploring the optical properties of holey fibers," in *Nanoscale Linear and Nonlinear Optics: International School on Quantum Electronics, Erice, Sicily, July 2000*, M. Bertolotti, C. M. Bowden, and C. Silbilia, Eds. Melville, NY: AIP, 2000, pp. 123–128.

[41] A. V. Husakou and J. Herrmann, "Supercontinuum generation in photonic crystal fibers made from highly nonlinear glasses," *Appl. Phys. B—Lasers Opt.*, vol. 77, pp. 227–234, 2003.
[42] A. W. Snyder and J. D. Love, *Optical Waveguide Theory*. London, U.K.: Chapman & Hall, 1983.
[43] M. H. Frosz, P. Falk, and O. Bang, "The role of the second zero-dispersion wavelength in generation of supercontinua and bright-bright soliton-pairs across the zero-dispersion wavelength," *Opt. Exp.*, vol. 13, pp. 6181–6192, 2005.
[44] M. L. V. Tse, P. Horak, F. Poletti, N. G. Broderick, J. H. V. Price, J. R. Hayes, and D. J. Richardson, "Supercontinuum generation at 1.06 microns in holey fibers with dispersion flattened profiles," *Opt. Exp.*, vol. 14, pp. 4445–4451, 2006.
[45] G. Q. Chang, T. B. Norris, and H. G. Winful, "Optimization of supercontinuum generation in photonic crystal fibers for pulse compression," *Opt. Lett.*, vol. 28, pp. 546–548, 2003.
[46] S. Coen, A. H. L. Chau, R. Leonhardt, J. D. Harvey, J. C. Knight, W. J. Wadsworth, and P. S. J. Russell, "Supercontinuum generation by stimulated Raman scattering and parametric four-wave mixing in photonic crystal fibers," *J. Opt. Soc. Amer. B—Opt. Phys.*, vol. 19, pp. 753–764, 2002.
[47] J. M. Dudley and S. Coen, "Coherence properties of supercontinuum spectra generated in photonic crystal and tapered optical fibers," *Opt. Lett.*, vol. 27, pp. 1180–1182, 2002.
[48] G. Genty, M. Lehtonen, H. Ludvigsen, J. Broeng, and M. Kaivola, "Spectral broadening of femtosecond pulses into continuum radiation in microstructured fibers," *Opt. Exp.*, vol. 10, pp. 1083–1098, 2002.
[49] R. H. Stolen, C. Lee, and R. K. Jain, "Development of the stimulated raman-spectrum in single-mode silica fibers," *J. Opt. Soc. Amer. B—Opt. Phys.*, vol. 1, pp. 652–657, 1984.
[50] R. H. Stolen, J. P. Gordon, W. J. Tomlinson, and H. A. Haus, "Raman response function of silica-core fibers," *J. Opt. Soc. Amer. B—Opt. Phys.*, vol. 6, pp. 1159–1166, 1989.
[51] J. P. Gordon, "Theory of the soliton self-frequency shift," *Opt. Lett.*, vol. 11, pp. 662–664, 1986.
[52] A. Efimov, F. G. Omenetto, A. J. Taylor, J. C. Knight, W. J. Wadsworth, and P. S. J. Russell, "Generation of UV light from microstructured fibers pumped with femtosecond 800 nm oscillator," presented at the Conf. Lasers Electro-Opt., Long Beach, CA, 2002, Paper CThL5.
[53] X. Feng, A. K. Mairaj, D. W. Hewak, and T. M. Monro, "Towards high-index glass based monomode holey fibre with large mode area," *Electron. Lett.*, vol. 40, pp. 167–169, 2004.

Jonathan H. V. Price (S'02–M'03) received the Ph.D. degree in optoelectronics from the Optoelectronics Research Centre, University of Southampton, U.K., in 2003.

He is currently a Royal Academy of Engineering Postdoctoral Research Fellow with the Optoelectronics Research Centre. His current research interests include novel microstructured optical fibers for ultrashort-pulse applications and the development of high-power femtosecond pulsed fiber laser sources.

Tanya M. Monro received the Ph.D. degree in optical physics from the University of Sydney, Sydney, Australia, in 1998.

She is currently the Director of the Centre of Expertise in Photonics, University of Adelaide, Adelaide, Australia, where she has been since 2005. Her current research interests include microstructured fibers, soft glasses, fibers for new transmission wavelengths, nonlinear fibers, and biological and chemical sensing.

Heike Ebendorff-Heidepriem received the Ph.D. degree in chemistry from the University of Jena, Jena, Germany, in 1994.

Since 2005, she has been the Deputy Director of the Centre of Expertise in Photonics, University of Adelaide, Adelaide, Australia. Her current research interests include optical glasses, spectroscopy of rare earth ions, glass flow behavior, and soft glass microstructured fibers.

Francesco Poletti received the Laurea Ing degree in electronics from the University of Parma, Parma, Italy in 2000.

He is currently a Research Fellow with the Optoelectronics Research Centre, University of Southampton, Southampton, U.K. His current research interests include numerical techniques for electromagnetic modeling, inverse design methods, nonlinear optics, and microstructured optical fiber design.

Peter Horak received the Ph.D. degree in theoretical quantum optics from the University of Innsbruck, Innsbruck. Austria, in 1997.

He is currently a Senior Research Fellow with the Optoelectronics Research Centre. His current research interests include theory and modeling of nonlinear pulse propagation, optical microcavities, and noise properties of optoelectronic devices.

Vittoria Finazzi received the Ph.D. degree in optoelectronics from the Optoelectronics Research Centre, University of Southampton, Southampton, U.K., in 2004.

She has been a Researcher with the Institute of Photonic Sciences (ICFO), Barcelona, Spain, since November 2006. Her current research interests include microstructured fibers, nanotapers, fiber gratings, and sensor applications.

Julie Y. Y. Leong received the B.Sc. degree (Hons.) in electrical and electronic engineering (first-class honors) from the University of Technology, Sarawak, Malaysia in 2001.

She is a Research Student with the Optoelectronics Research Centre. Her current research interests include the fabrication and applications of nonsilica microstructured optical fibers.

Periklis Petropoulos received the Ph.D. degree in optical telecommunications from the Optoelectronics Research Centre, University of Southampton, Southampton, U.K., in 2000

He has been with the Optoelectronics Research Centre. Since 1996, where he is currently a Reader. His current research interests include all-optical processing and switching in optical fibers, pulse manipulation for optical communications using fiber Bragg gratings including applications in optical correlation systems for the implementation of optical code division multiple access and optical packet switched systems, applications of silica and compound glass holey fibers, and fiber lasers.

Joanne C. Flanagan received the Ph.D. degree in optoelectronics from the Optoelectronics Research Centre, University of Southampton, Southampton, U.K., in 2000.

She is currently a Research Fellow with the Optoelectronics Research Centre. Her current research interests include numerical techniques for electromagnetic modeling, and the design and applications of microstructured optical fibers.

Gilberto Brambilla received the Ph.D. degree in optoelectronics from the Optoelectronics Research Centre, University of Southhampton, Southhampton, U.K. in 2001.

He is currently a Senior Research Fellow with the Optoelectronics Research Centre, since 1998. His current research interests include optical fiber nanowires, photosensitivity, radiation fiber sensors, specialty fibers, and glass technology.

Xian Feng received the Doctor of Engineering degree in material science from the Shanghai Institute of Optics and Fine Mechanics, Chinese Academy of Sciences, Shanghai, China, in 1999.

He is currently a Senior Research Fellow with the Optoelectronics Research Centre. His current research interests include the fabrication and applications of nonsilica microstructured optical fibers.

David J. Richardson received the Ph.D. degree in fundamental physics from Sussex University, Sussex, U.K., in 1989.

He is currently a Deputy Director of the Optoelectronics Research Centre, University of Southampton, Southampton, U.K., since 1989. His current research interests include microstructured fibers, high-power fiber lasers, short-pulse lasers, optical fiber communications, and nonlinear fiber optics.